Free energy, energy, and entropy of swelling in Cs–, Na–, and Sr–montmorillonite clays

Heather D. Whitley and David E. Smith
*Department of Chemistry and Biochemistry, MSC 3C, New Mexico State University, P.O. Box 30001,
Las Cruces, New Mexico 88003-8001*

A Monte Carlo method for grand canonical and grand isoshear ensemble simulations has been used to characterize the free energy, energy, and entropy of clay mineral swelling. The Monte Carlo approach was found to be more efficient at simulating water content fluctuations in the highly constrained clay environment than a previously developed molecular dynamics method. Swelling thermodynamics calculated for Cs–, Na–, and Sr–montmorillonite clays indicate a strong dependence of swelling on the interlayer ion identity, in agreement with various experimental measurements. The Sr clay swells most readily, and both the Na and Sr clays prefer expanded states (two-layer hydrate or greater) when in contact with bulk water. In contrast, swelling is inhibited in the Cs clay. Differences in swelling behavior are traced directly to the tendency of the different ions to hydrate. The swelling free energies are decomposed into their energetic and entropic components, revealing an overall energetic driving force for the swelling phenomena. Entropic effects provide a smaller, mediating role in the swelling processes. The results provide a unique molecular perspective on experimentally well-characterized swelling phenomena. © *2004 American Institute of Physics.* [DOI: 10.1063/1.1648013]

I. INTRODUCTION

Swelling and hydration of smectite clay minerals impact a variety of environmental and engineering processes. These include binding and bioavailability of ionic nutrients and pollutants, hydraulic conductivity of engineered containment materials, and borehole stability in petroleum drilling operations.[1–5] Practical concerns such as these have led to extensive experimental[6–16] and theoretical[17–31] investigations of swelling clays.

The equilibrium layer spacing for a smectite clay is a function of several thermodynamic and compositional variables. Key thermodynamic variables include the temperature, applied pressure, and water chemical potential, with the chemical potential controlled by the relative humidity or solution ionic strength. Important compositional variables include the magnitude and location of the negative clay layer charge and the identity of the charge-balancing cations that reside in the interlayer. Of these variables, the interlayer cations play a particularly interesting role. For example, the Na-, Cs-, and Sr-substituted smectites considered in this paper show significantly different swelling behavior.[10,11] Cs^+ is a swelling inhibitor, preventing the formation of swelling states beyond a single water layer. In contrast, Sr and Na smectites both swell readily to multilayer hydrates, with the Na clays swelling even to macroscopic spacings under appropriate thermodynamic conditions.

Crystalline or short-range swelling of smectite clay minerals may be described in terms of a series of layer-spacing transitions that are thermodynamically analogous to phase transitions. Swelling occurs in a discrete fashion, through the stepwise formation of integer-layer hydrates or mixtures thereof. The mixed-layer hydrates have an average layer spacing intermediate between two adjacent integer-layer states and correspond thermodynamically to a "phase coexistence" of those two states. The equilibrium layer spacing for a clay is the state in which the thermodynamic potential or "free energy" is a global minimum at that system's temperature, pressure, and water chemical potential. There may be multiple local minima in the thermodynamic potential associated with different integer-layer states. Trapping in these metastable local minima is one likely origin of hysteresis commonly associated with crystalline swelling processes.

Computer simulation methods and molecular theories can provide unique information on crystalline swelling of clay minerals and other layered systems. Unlike in experimental measurements, computational and theoretical methods can reveal the entire swelling potential, or free energy, including both stable points and transition regions. Decomposition of swelling free energies into entropic and energetic components is also possible, providing significantly improved understanding of the origins of observed swelling behavior. Finally, since detailed structural information is directly accessible from computational and theoretical investigations, these methods have great potential in identifying important structure-function relationships for clay swelling processes.

Simulations in the grand canonical or related ensembles are required for prediction of the equilibrium spacing or water content of a given clay. A variety of grand canonical simulation techniques have been described.[32,33] We recently reported a grand canonical molecular dynamics (MD) simulation of the swelling of Cs–montmorillonite.[22] Lengthy simulations revealed a noisy disjoining pressure curve. Integration of the disjoining pressure yielded the free energy,

TABLE I. Interaction potential parameters for SPC/E water.

Element	σ (Å)	ϵ (kJ/mol)	q/e
O	3.166	0.650	−0.848
H	0.000	0.000	0.424
Cs	3.830	0.418	1.000
Na	2.350	0.544	1.000
Sr	3.341	0.418	2.000

TABLE II. Interaction potential parameters for clay.

Layer	Element	σ (Å)	ϵ (kcal/mol)	q/e
Tetrahedral	O	3.166	0.650	−0.800
	Si	1.804	13.18	1.200
Apical	O	3.166	0.650	−1.000
Octahedral	O	3.166	0.650	−1.424
	H	0.000	0.000	0.424
	Al	0.000	0.000	3.000
	Mg	0.000	0.000	2.000

with minima observed as expected for both the one- and two-layer hydrates. However, the swelling free energy indicated incorrectly that Cs–montmorillonite favors the two-layer hydrate. It was unclear whether this conclusion was a proper representation of the model or an artifact of large simulation uncertainties. Subsequently, Mezei demonstrated that a grand canonical Monte Carlo (MC) method is much more efficient than our grand canonical MD method for simulations of water.[34] His results suggest strongly that a MC approach could prove to be more productive in treating clays as well.

In this article, we report results of grand isoshear ensemble simulations of hydrated Na–, Cs–, and Sr–montmorillonite clays. The MC approach to these simulations was found to be significantly more efficient than our previous MD implementation. Disjoining pressures and swelling free energies were calculated for the three clays and showed good agreement with experimental swelling measurements. Structural analysis highlighted an important role for the formation of primary ion hydration shells in the swelling process. Swelling free energies were decomposed into energetic and entropic components, revealing a predominantly energetic origin for swelling and a smaller, compensating role for entropy. Finally, disjoining pressures for Na–montmorillonite were analyzed to predict how equilibrium layer spacing depends on external pressure and how trapping in metastable states leads to swelling hysteresis.

II. COMPUTATIONAL METHODS

A. Model and potentials

The solution and clay interaction potentials used here are identical to those described previously.[21–23] Water is represented by the "extended" simple point charge (SPC/E) model of Berendsen and co-workers.[35] Each water molecule consists of three interaction sites located at the atomic nuclei. These molecules have a rigid geometry with a bond length of 1 Å and a tetrahedral bond angle of 109.47°. A Lennard-Jones (LJ) potential and partial charges on the atomic sites govern the intermolecular interactions. Parameters for the model are given in Table I. The permanent dipole moment of the SPC/E water (2.35 D) is enhanced compared to the experimental gas phase value (~1.85 D) in order to mimic the polarization of water in the liquid state. This representation of the induced dipole by a permanent dipole necessitates the inclusion of a self-polarization correction to both the energy and free energy of water.[35,36] The Cs^{+}, Na^{+}, and Sr^{2+} ions are similarly modeled with a point charge plus LJ potential, with parameters also shown in Table I. All LJ cross interaction terms are generated from the combining relationships

$$\sigma_{ij}=\frac{1}{2}(\sigma_i+\sigma_j), \tag{1}$$

$$\epsilon_{ij}=(\epsilon_i\epsilon_j)^{1/2}. \tag{2}$$

The simulation model for clay used here is closely related to the empirical models of Skipper and co-workers[17,37,38] and is described in greater detail elsewhere.[21] The clay is represented by a rigid lattice, the coordinates of which were determined from x-ray diffraction studies of the uncharged mineral talc.[39] Partial charges and LJ parameters were assigned to each atomic site in the clay, with parameters given in Table II. The parameters for oxygen and hydrogen atoms in the clay are equivalent to those used in water. The clay model was modified from that of Skipper *et al.* to achieve consistency with the SPC/E water model and to provide uniform LJ-type parametrization of the van der Waals interactions. The specific clay modeled here is a member of the montmorillonite class of smectite clay minerals and has a layer charge of −0.75e located exclusively in the octahedral sheet. The unit-cell formula of the clay is therefore

$$X_{0.75/n}^{+n}[Si_8](Al_{3.25}Mg_{0.75})O_{20}(OH)_4$$
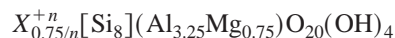
where X represents the interlayer ion (Cs, Na, or Sr) and n is the charge of the ion. Tetrahedral substitution sites in this model have been shown to yield qualitatively incorrect ion exchange free energies and were therefore not included in this study.[40]

The total potential energy for the system is given by summations over all interaction sites,

$$U=\sum_i \sum_j {}' \left\{4\epsilon_{ij}\left[\left(\frac{\sigma_{ij}}{r_{ij}}\right)^{12}-\left(\frac{\sigma_{ij}}{r_{ij}}\right)^6\right]+\frac{q_iq_j}{r_{ij}}\right\}, \tag{3}$$

where the prime denotes the exclusion of intramolecular interactions. The self-polarization energy correction for water is included implicitly. All short-range interactions are truncated using a minimum-image convention, while the long-range Coulombic contribution to the potential energy is determined using the Ewald summation method.[32,41]

B. Grand canonical and grand isoshear methods

Simulations in the grand canonical ensemble were performed using both MD and MC approaches. A grand canonical molecular dynamics (GMD) simulation method was developed previously in our group and used to determine the swelling free energy of a Cs–montmorillonite clay.[22,36] In this method, particle insertions and deletions are accom-

plished in a continuous fashion through the use of a fractional particle and a continuous particle-number variable. This approach was motivated in part by the hope that gradual insertion and deletion processes would lead to more efficient particle fluctuations than produced in grand canonical Monte Carlo (GCMC) simulations. Recently, Mezei compared the efficiency of our GMD approach with his cavity-biased GCMC method.[34] Using a simulation of pure water and our reported GMD results,[36] he concluded that GCMC is significantly better at sampling particle fluctuations. In order to investigate efficiency issues further, we have developed a GCMC implementation for our code that allows for direct comparison of GMD and GCMC methods in the highly constrained clay interlayer environment.

In our GCMC approach, a random number is used at each step to determine whether a particle displacement, deletion, or insertion will be attempted. The probabilities for selecting displacement and deletion attempts are kept equal. Insertion attempts are computationally cheaper than deletions as most trials may be rejected using distance criteria without a full energy calculation. We have therefore used an enhanced probability for insertion attempts. The probabilities for insertions (P_i) and deletions (P_d) are related by

$$r_{id} = \frac{P_i}{P_d}, \quad (4)$$

where r_{id} may be adjusted to optimize computational efficiency. In a particle displacement step, a random particle is selected and a trial translation and rotation is attempted. Acceptance of the move is determined by the usual Metropolis criterion.[33] For insertions, a trial particle with random position and orientation is placed into the system. For clay simulations, its z-coordinate position is restricted to be within the interlayer region, 3.9 Å or more from the center of each clay layer. Insertions that yield minimum O–O distances of less than 2.3 Å or minimum ion–O distances of less than 2.05, 2.60, and 2.35 Å for Na^+, Cs^+, and Sr^{2+} ions, respectively, are rejected without performing a full energy calculation. Molecules are never observed to be within these distances in canonical ensemble simulations. Insertions of molecules that pass these simple distance criteria are accepted with probability

$$P_{acc}^{N \rightarrow N+1} = \min\left[1, \frac{V}{r_{id}\Lambda^3(N+1)} \exp[\beta(\mu - \Delta U)]\right], \quad (5)$$

where Λ is the thermal de Broglie wavelength for water, $\beta = 1/k_B T$, μ is the target chemical potential, and ΔU is the change in the total energy of the system following the insertion. The volume V corresponds to the simulation box volume minus the volume of the excluded clay region. For deletions, a random particle is selected for removal. The deletion is accepted with probability

$$P_{acc}^{N+1 \rightarrow N} = \min\left[1, \frac{r_{id}\Lambda^3(N)}{V} \exp[-\beta(\mu + \Delta U)]\right], \quad (6)$$

where the symbols are defined as above. While this GCMC implementation does not include more elaborate cavity-bias
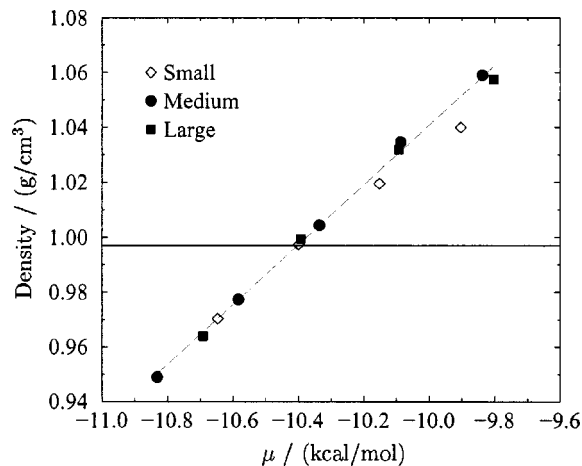
FIG. 1. Water density plotted as a function of total chemical potential μ for systems with box lengths of 14.80 Å (small), 18.64 Å (medium), and 23.49 Å (large). The dashed line is a linear regression fit of the medium and large system data. It crosses the experimental water density (0.997 g/cm^3, solid line) at a chemical potential of -10.40 kcal/mol.

or configuration-bias methods,[42,43,27] it should still provide a useful base line for comparing GMD and GCMC methods in clay mineral simulations.

The probability ratio for insertion and deletion attempts was optimized using a criterion similar to Shelley and Patey's.[43] In this method, the average number of deletions per unit CPU time, n_t, is optimized with respect to r_{id}. Particles present in the system for fewer than 100 000 MC cycles are not included in the average since deletion of recently inserted particles is likely unproductive with respect to long-term particle number fluctuations. Each MC cycle corresponds to $r_{id} + 2$ MC steps or, on average, one attempted displacement, one attempted deletion, and r_{id} attempted insertions. Values of $r_{id} = 30$ and $r_{id} = 50$ were found to be nearly optimal for bulk water and clay, respectively, and were used in reported simulations of water, Sr–, and Na–montmorillonite. Cs–montmorillonite simulations were also performed with $r_{id} = 50$, but in addition to these simulations, some Cs–montmorillonite simulations were completed using a value of $r_{id} = 1$. The results did not vary significantly for the different values of r_{id}. All of the results from the Cs–montmorillonite simulations are included in our data.

Simulations of bulk SPC/E water were used both to validate the GCMC method and to determine precisely the bulk SPC/E water chemical potential. For temperatures near 298 K and an excess chemical potential of -5.7 kcal/mol, it is known that SPC/E water has a density near the experimental value of 0.997 g/cm^3 (Refs. 36, 43, and 44). Adding the ideal chemical potential (translational contribution only) to this value yields a total chemical potential of -10.3 kcal/mol. Simulations were performed on three systems with box lengths of 14.798, 18.644, and 23.491 Å (labeled small, medium, and large, respectively). The sizes were chosen such that water contents of 108, 216, and 432 molecules, respectively, correspond to the experimental water density. Results are presented in Fig. 1. The values of the chemical potential all include corrections for the self-polarization free energy
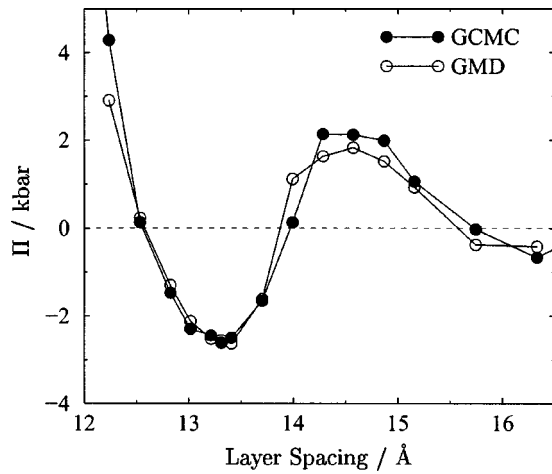
FIG. 2. Comparison of Cs–montmorillonite disjoining pressures calculated using GCMC and GMD methods. The graph is displayed only over the limited range of spacings for which both methods were used.

(1.25 kcal/mol) and a small tail correction for the LJ energies of molecules outside the simulation box.[36] The data indicate that the density varies nearly linearly with chemical potential over the simulated range. Linear regression of the medium and large system results yields a bulk (0.997 g/cm^3) chemical potential of -10.40 kcal/mol, in good agreement with previous measurements.[36,43,44] The small system results were not included in the regression analysis since they reveal a possible system-size dependent density at the higher chemical potentials. The slope of the plot in Fig. 1 may be related to the isothermal compressibility κ_T through

$$\left(\frac{\partial \rho}{\partial \mu}\right)_{T,V} = \frac{\rho^2 \kappa_T}{M}, \tag{7}$$

where ρ is the mass density and M is the molar mass of water. Analysis of the slope yields a value of κ_T of 4.7 $\times 10^{-5}$ bar^{-1}, in excellent agreement both with the experimental value of 4.5×10^{-5} bar^{-1} and with a previously reported value of 5×10^{-5} bar^{-1} for SPC/E water.[45]

Simulations of hydrated clay minerals were performed in the grand isoshear ensemble, with thermodynamic shear forces set to zero. These calculations make use of the grand canonical method described above but with an additional step for relaxation of the clay registry (x,y) coordinates.[22,46,47] Random lateral movement in the x and y directions between -0.1 Å and 0.1 Å are attempted for one clay sheet every 500 MC cycles, with acceptance of the registry moves based on the standard Metropolis criterion.[32]

The grand isoshear MD and MC methods were compared by calculating several properties of a Cs–montmorillonite clay. All the results from the two methods were in good agreement. For example, disjoining pressure curves calculated from the two methods are displayed in Fig. 2. The total CPU time for each MC point in the figure is approximately 1/4 of that for the comparable MD point. Nevertheless, the two curves have similar shapes and apparent noise levels. This suggests that the MC approach is more efficient than the current MD implementation.

The particle insertion and deletion efficiencies of the MD and MC methods were quantified by comparing their relative n_t values, where n_t is defined as described above in the r_{id} optimization. In the MD method, many inserted particles are subsequently removed without ever achieving the status of a "full" particle. These deletion events are unproductive with respect to particle-number fluctuations and were therefore not included in the n_t calculation. In the MC method, n_t was calculated as described above. The ratios of the MC to MD n_t values for several different clay-layer spacings were in the range of 100–200. The MC method therefore has a clear efficiency advantage over the MD method at least with respect to sampling of particle fluctuations. This confirms that Mezei's observation[34] of MC superiority in simulations of pure water also holds true in the constrained clay interlayer environment.

C. Swelling thermodynamics

Thermodynamic expressions for swelling in slit pore environments have been derived previously.[22,46,47] Under thermodynamic constraints of constant temperature, water chemical potential, applied shear stresses, and normal applied stress, the clay swelling "free energy" is given by

$$\Delta X = X(s_z) - X(s_z^0) = A \int_{s_z^0}^{s_z} [T_{zz}(s_z') - T_{zz}'] ds_z', \tag{8}$$

where s_z is the layer spacing, A is the area of the clay sheet, and T_{zz}' is the constant, external stress applied normal to the clay sheets. In this work, the normal internal stress (T_{zz}) is evaluated using the expression

$$T_{zz} = -kT \frac{\langle N_{\text{int}} \rangle}{V} + \frac{1}{A} \left\langle \left(\frac{\partial U}{\partial s_z}\right) \right\rangle, \tag{9}$$

where $\langle N_{\text{int}} \rangle$ is the average number of interlayer water molecules and ions and U is the system potential energy. Averages in this expression are determined as a function of layer spacing using a series of grand isoshear ensemble simulations, with the partial derivative in the second term evaluated using a finite-difference scheme. The applied stress T_{zz}' is equal to $-p_b - p_z^{\text{ext}}$, where p_b is the bulk (isotropic) solution pressure and p_z^{ext} is the external pressure applied normal to the clay sheets, but *not* to the adjoining aqueous solution. Substitution of these quantities into Eq. (8) yields

$$\Delta X = -A \int_{s_z^0}^{s_z} [\Pi(s_z') - p_z^{\text{ext}}] ds_z', \tag{10}$$

where the "disjoining pressure" Π is equal to $-T_{zz} - p_b$.

The swelling free energy (X) is related to the internal energy through several Legendre transformations,

$$X = E - TS - \mu N - T_{zz}As_z - T_{xz}Al_x - T_{yz}Al_y, \tag{11}$$

where the last two terms are related to the applied shear stresses. Differentiating this equation with thermodynamic constraints of constant T, μ, and $T_{zz} = -p_b$ and assuming zero applied shear forces yields

$$\Delta X = \Delta E - T\Delta S - \mu \Delta N + p_b A \Delta s_z. \tag{12}$$

If the adjoining aqueous solution is pure water, the chemical potential μ is equal to the molar Gibbs energy of water,

$$\mu = \frac{G}{n} = E_m - TS_m + p_b V_m, \qquad (13)$$

where the m subscript indicates molar quantities. Substituting this expression for μ into Eq. (12) yields

$$\Delta X = (\Delta E - E_m \Delta N) - T(\Delta S - S_m \Delta N)$$
$$+ p_b(A \Delta s_z - V_m \Delta N). \qquad (14)$$

The first two terms in this equation correspond to the energy and entropy changes, respectively, for the composite clay plus bulk water system. The final term in the equation is a similar composite "pV" energy and is very small at a pressure of $p_b = 1$ bar. Representing the composite energy and entropy changes by ΔE^c and ΔS^c and neglecting the final "pV" term yields the simplified expression

$$\Delta X = \Delta E^c - T \Delta S^c. \qquad (15)$$

This equation provides a mechanism for identifying energy and entropy contributions to the clay swelling process. ΔX is determined from the integral of the disjoining pressure [Eq. (10)], and the composite energy change ΔE^c is calculated from the clay and bulk water simulation energies. The difference between these two terms yields the composite entropy contribution $-T \Delta S^c$ to the clay swelling process.

Our goal in decomposing the swelling free energy into its entropic and energetic components is to provide improved understanding of the thermodynamic origins of clay swelling behavior. Entropy is often also related to the temperature dependence of a process. This is not true for ΔS^c, however, since it is calculated assuming a constant value for the chemical potential of water. In fact, μ has a large temperature dependence that contributes significantly to the temperature dependence of clay swelling.

D. Simulation details

The simulation system is composed of a periodically replicated rectangular prism with x- and y-axis lengths of 21.12 Å by 18.28 Å. The system includes two clay layers each containing eight clay unit cells. The charge-balancing cesium, sodium, or strontium ions are distributed equally between the two interlayer regions. The z axis is perpendicular to the clay sheets and its length is chosen to yield the desired interlayer volume. The volume of each of the two interlayer regions is constrained to be equal and is held constant during the course of each simulation. Equilibrium configurations were generated with clay layer spacings ranging between 12.0 Å and 18.5 Å, where reported spacings include the ~10 Å thickness of the clay lattice. The water-accessible, interlayer widths therefore ranged between about 2.0 and 8.5 Å.

Equilibrium starting configurations for the MC simulations were generated as follows. A few initial configurations for the Na^+ and Sr^{2+} substituted clays were taken from previous Cs–montmorillonite MD simulations.[22] For the Sr clay, half of the Cs^+ ions were removed in order to maintain charge neutrality. In most cases, initial configurations were
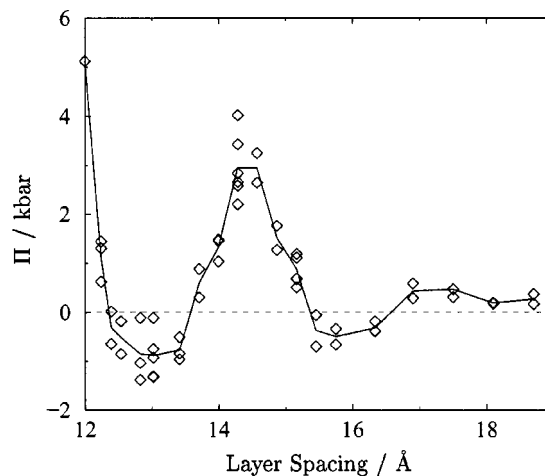
FIG. 3. Disjoining pressure for Na–montmorillonite. The solid line is the average of the individual pressure points.

generated by adjusting the layer spacing in previously equilibrated systems containing the same interlayer ion. In every case, the number of water molecules in the initial configuration was reduced by 50 and a canonical ensemble simulation at high temperature (5000 K) was performed for 1×10^5 MC cycles. This served to randomize ion, water, and registry positions. The high-temperature runs were followed by a grand isoshear ensemble annealing process in which the target temperature was reduced gradually from 1000 K to 298.15 K over a period of 5×10^5 MC cycles. The water contents for each spacing fluctuated significantly during the annealing process, but approached their equilibrium values as the simulations reached room temperature. Following annealing, each system was allowed to equilibrate for between 5×10^5 and 2.5×10^6 cycles, depending on the layer spacing.

For each system, production runs were performed for between 1×10^7 and 3×10^7 MC cycles depending on system size. The simulation duration was chosen to assure that at least 1×10^5 displacements were attempted per water molecule. Averages were collected for the energy, water content, pressure, and various structural quantities.

III. RESULTS AND DISCUSSION

The disjoining pressures calculated for Na–montmorillonite are displayed in Fig. 3. Data points from independent simulations are indicated with symbols, with the solid line corresponding to averages of the individual points at each spacing. This plot gives an indication of the noise in individual pressure calculations. The noise seen in the plots for Sr– and Cs–montmorillonite (not shown) is similar to that for Na–montmorillonite.

The average disjoining pressures for Cs–, Na–, and Sr–montmorillonite are displayed in Fig. 4. The disjoining pressure curves for the three clays are qualitatively similar, exhibiting oscillations around the zero kbar line. Mechanically stable states for these systems correspond to the points where the disjoining pressure curve has a negative slope and a value equal to the external pressure applied normal to the clay sheets.[22] Stable states are identified for the Na–montmorillonite at 12.4 and 15.4 Å, for Cs–montmorillonite
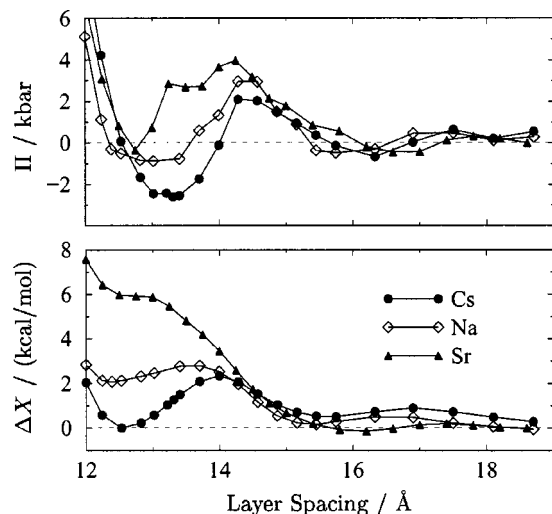
FIG. 4. Average disjoining pressures (top) and swelling free energies (bottom) for Cs–, Na–, and Sr–montmorillonite.

FIG. 5. Ion–water hydration numbers (top) correlated with average disjoining pressures (bottom) for Cs–, Na–, and Sr–montmorillonite.

at 12.6 and 15.7 Å, and for Sr–montmorillonite at 12.7 and 16.1 Å. States with approximately these spacings are commonly referred to as one-layer and two-layer hydrates, respectively. Additional three-layer hydrate states may occur in the ≈18–19-Å region for all clays, but these features are obscured by noise in the data. At the smallest spacings, the Cs–montmorillonite pressure is greater than that for Sr– or Na–montmorillonite due to the larger size of the Cs ions. The curves for Na and Cs cross at about 12.7 Å, with the Cs-clay pressures remaining significantly lower than the Na-clay pressures for spacings up to around 15 Å. The Sr and Cs curves cross at about 12.4 Å, and both the Cs- and Na-clay pressures remain significantly below those for Sr clay out to around 15 Å. Beyond this spacing, the three clays behave similarly.

Variations in disjoining pressure lead to significant differences in swelling free energies for the three clays, also displayed in Fig. 4. The swelling free energy is determined by integration of the disjoining pressure [Eq. (10)] assuming a value of $p_z^{ext}=0$. The reported free energy values have also been divided by 6, the magnitude of the layer charge in one clay sheet in our system, in order to give values independent of system size. The stable states discussed above correspond to minima in this free energy. Higher pressures in the 12.5–15-Å region destabilize the one-layer hydrate relative to the two-layer hydrate. As a result, the Cs–montmorillonite is the only one of the three clays with an equilibrium one-layer state. In contrast, the expanded states (two- and three-layer hydrates) are preferred for Sr– and Na–montmorillonite. The disjoining pressures in the Sr clay are so large that the one-layer hydrate is essentially a high-energy plateau rather than a true minimum.

Equilibrium layer spacings predicted from the simulations for Cs–montmorillonite (12.6 Å), Na–montmorillonite (15.4 Å), and Sr–montmorillonite (16.1 Å) may be compared with both experimental and other simulation measurements. At room temperature and 100% relative humidity, Cs–montmorillonite exist as one-layer hydrates with reported layer spacings ranging from from 12.2 to 12.9 Å.[6,7,10,13] Un-

der the same conditions, Na–montmorillonites may exist as two-layer, three-layer, or even in fully expanded states depending upon the preparation method and precise clay composition. Two-layer hydrate spacings have been reported to range from 15.2 to 15.8 Å.[6–8,10,13,14] For Sr–montmorillonite, Cases et al.[11] reported a layer spacing of 15.8 Å for a clay of similar composition to ours. It is clear that all of these experimental measurements are in good agreement with our simulation predictions. Our predicted layer spacing also agrees well with previous grand canonical simulation results for Na–montmorillonite.[24] The relative stabilities of the one- and two-layer hydrates for Cs–montmorillonite are reversed from those in our previous work,[22] possibly due to differences in the treatment of registry motions or to a better signal-to-noise ratio in the current study.
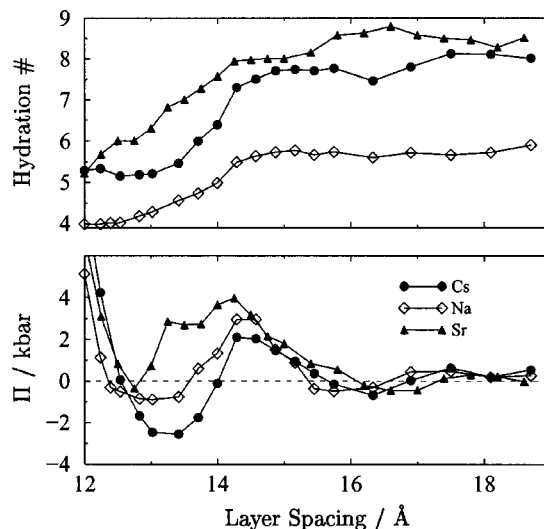
Cs–, Na–, and Sr–montmorillonite disjoining pressures are compared with average ion hydration numbers in Fig. 5. Average hydration numbers were determined by integration over the first solvation shell in the ion–oxygen pair correlation functions that were calculated for the interlayer solutions. Clay surface oxygen atoms were not included in the hydration numbers. The spatial extent of the first solvation shell was defined to be 3.15 Å for Na^+, 4.00 Å for Cs^+, and 3.50 Å for Sr^{2+}, corresponding to the first minimum in the pair correlation functions calculated from clays with the largest spacings. At large spacings, the ion hydration numbers approach their bulk SPC/E water values of 6.0, 8.4, and 8.5 for Na^+, Cs^+, and Sr^{2+}, respectively. The largest oscillation in each disjoining pressure curve is clearly correlated with the ion hydration number. In particular, in the 13–16-Å region, increasing pressures are associated with increasing hydration numbers, while decreasing pressures correspond to relatively flat hydration numbers. These data suggest that the stable spacings and relative stabilities of one- and two-layer hydrates are determined primarily by the formation of ion hydration shells. The larger disjoining pressures for Sr^{2+} and Na^+ in this region result from their stronger abilities to form
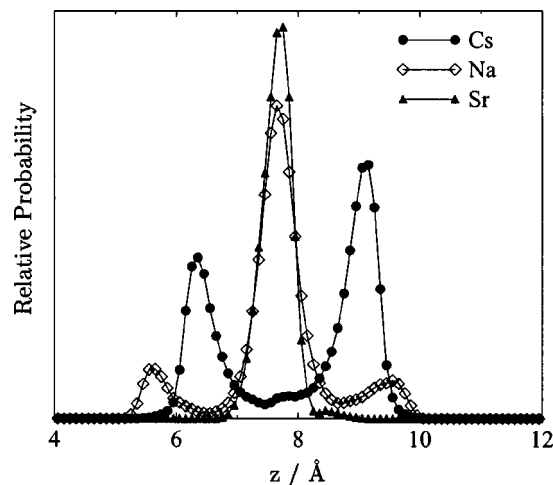
FIG. 6. Ion density profiles for Cs–, Na–, and Sr–montmorillonite two-layer hydrates (layer spacing=15.45 Å), where z corresponds to the distance from the middle of the central clay layer.

FIG. 7. Water–oxygen density profiles for three Na–montmorillonite hydrates, where z corresponds to the distance from the middle of the central clay layer.

complexes with water molecules. This in turn destabilizes the one-layer hydrate relative to the two-layer state.

Interlayer ion position is also correlated with ion hydration energy. Ion density profiles for the three montmorillonites with spacings of 15.45 Å (approximately two-layer hydrates) are displayed in Fig. 6. While Cs–montmorillonites are not observed experimentally at this spacing, it is instructive to compare the behavior of the three ions under similar geometric constraints. Density profiles indicate that the Cs^+ ion has a strong preference to form "inner-sphere" complexes close to the clay surface and with a more limited hydration shell than it could obtain with a central placement. Interestingly, its hydration number is 7.7 in this clay compared to a bulk water value of 8.4, so its overall reduction in hydration number upon inner-sphere formation is quite modest. The Sr^{2+} ion exhibits the opposite behavior from Cs^+, forming exclusively "outer-sphere" complexes. The Na^+ ion shows intermediate behavior, with significant population in both inner-sphere and outer-sphere configurations and a preference for the latter. The trend that emerges from the ion density profiles is that increasing hydration energy precludes the formation of inner-sphere complexes. This is not surprising since the formation of such complexes necessarily involves the shedding of some first shell waters of hydration.

The observation that stable swelling states in clays are determined by ion hydration structures rather than by layering of water molecules suggests that the "one-layer" and "two-layer" hydrate terminology commonly used in discussions of crystalline swelling may be misleading or even incorrect. On the other hand, hydrated ion sizes are intimately related to the molecular size of water, so the language may be appropriate regardless of the source of the discrete layering. To investigate this further, interlayer water density profiles were calculated for the thermodynamically stable states of each clay. Results for the Na–montmorillonite are displayed in Figs. 7. The density plot for the 12.39-Å spacing shows a single peak with a small splitting. The plots for the 15.45-Å and 18.10-Å spacings show two and three distinct density peaks, respectively. Results for Sr– and Cs–
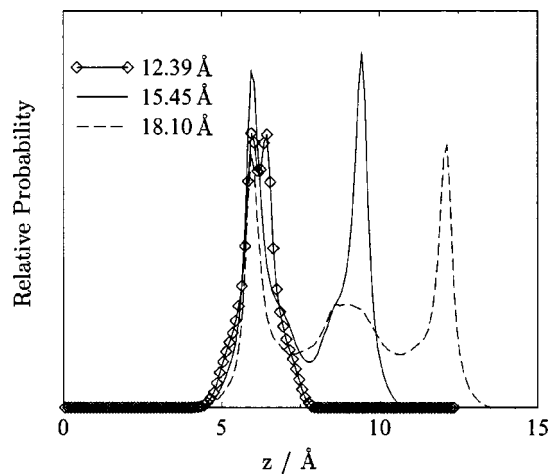
montmorillonite (not shown) are similar except that the splittings in the one-layer hydrate peaks are somewhat more pronounced. It is clear from these observations that well-defined water layers do exist in each of these hydrates, suggesting that the integer-layer terminology is indeed appropriate.

Interlayer ion and water density profiles in vermiculite clay minerals have been determined using neutron diffraction techniques.[48–50] Vermiculite clays vary significantly from montmorillonites in both layer charge magnitude and location. Nevertheless, their well-characterized interlayer structures provide a valuable qualitative comparison with structures predicted in simulations. Water density profiles in one-layer (11.78 Å) and two-layer (14.96 Å) hydrates of a Na–vermiculite[48] are very similar to those displayed in Fig. 7 except that splitting in the one-layer hydrate peak is not observed. This splitting disappears in the Na–montmorillonite simulations as the layer spacing is reduced to 12.00 Å. Diffraction measurements also suggest that Na^+ ions may form either inner-sphere or outer-sphere complexes in two-layer hydrates, but that Li^+ and Ni^{2+} ions form exclusively outer-sphere complexes under the same conditions.[48,50] This is consistent with the trends identified in Fig. 6.

The thermodynamic origins of the clay swelling properties identified above may be investigated by decomposing the swelling free energies into their energetic and entropic components, following Eq. (15). The resulting composite-system energies (ΔE^c) and entropies ($-T\Delta S^c$) are displayed in Fig. 8 for Na–, Cs–, and Sr–montmorillonite. All three clays show qualitatively similar behavior. Most notably, the relative stabilities of one- and two-layer hydrates in each clay clearly have an energetic origin, as do the free energy barriers between the one- and two-layer hydrates in the Cs and Na clays. In addition, the energetic and entropic contributions to the free energy appear to be generally opposite. As the energy increases in the barrier regions, there is a corresponding decrease in $-T\Delta S^c$. When the energy decreases, the entropy term increases. This "energy–entropy compensation" is commonly observed[51,52] and can result
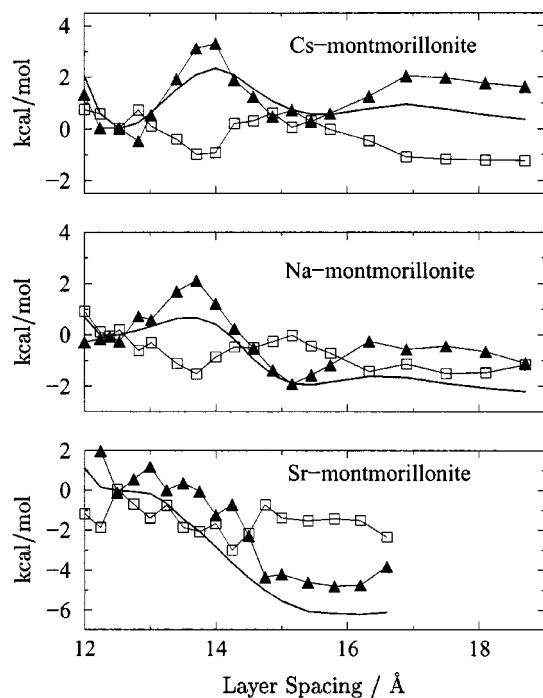
FIG. 8. Swelling free energy (thick solid lines) plotted along with composite system energy (ΔE^c, triangles) and entropy ($-T\Delta S^c$, squares) for Cs–, Na–, and Sr–montmorillonite. All values are set to zero arbitrarily at $z \approx 12.5$ Å.

FIG. 9. Top: swelling free energies of Na–montmorillonite at applied pressures ranging from 0.0 to 1.2 kbar in 0.2 kbar increments. Pressure increases in the direction of the arrow. For ease of comparison, the one-layer hydrate free energy is assigned a value of zero for each pressure. The two-layer hydrate is more stable than the one-layer state for pressures below ≈ 0.7 kbar, while the situation is reversed at higher pressures. Bottom: applied pressure plotted versus layer spacings. Equilibrium layer spacings (solid lines) correspond to the free energy minima in the top plots. The horizontal line connects the one-layer and two-layer states at the coexistence pressure of 0.7 kbar. Dotted lines follow a hypothetical compression and expansion cycle that exhibits hysteresis due to trapping in metastable layer spacings (dashed lines).

from the fact that more energetically favorable states often have less configurational freedom. Although the energy and entropy are in competition, the energetic contribution to the free energy is dominant and the shapes of the energy and free energy curves are therefore qualitatively similar. This dominance of energy confirms that differences in clay swelling behavior, including, for example, the function of Cs^+ as a swelling inhibitor, may be traced directly to the relative hydration energies of the different interlayer ions. While often anticipated, this conclusion has previously received little direct confirmation.

The disjoining pressures displayed in Fig. 4 may also be used to predict how clay layer spacing depends on the external pressure p_z^{ext}. Recall that this pressure is applied perpendicular to the clay sheets, but *not* to the bulk solution. As a result, the water chemical potential is not affected by p_z^{ext} and the same set of disjoining pressures can therefore be used for each of its values. Swelling free energies for Na–montmorillonite were calculated using Eq. (10) and p_z^{ext} values ranging between 0.0 and 1.2 kbar. Results are displayed in Fig. 9. As expected, the free energy minima corresponding to both one- and two-layer hydrates shift inward slightly as the external pressure is increased, and the two-layer hydrate is destabilized relative to the one-layer state. The coexistence pressure for the two states is found to occur at a pressure of about 0.7 kbar. Compression and expansion pathways are also displayed in the bottom portion of the figure. Solid lines indicate the equilibrium layer spacings, with a transition to the one-layer hydrate occurring at the coexistence pressure. Trapping in metastable swelling states is possible for this process, leading to hysteresis. This is represented by the dotted lines in the figure. Clay swelling processes in nature and

in the laboratory are most commonly controlled by changing the water chemical potential rather than the external pressure. Hysteresis in these processes likely has a similar origin to that shown in Fig. 9 except that changes in the chemical potential lead to shifts the disjoining pressure itself rather than in the external pressure. This was illustrated recently in the work of Hensen and Smit.[28]

IV. CONCLUSION

Following Mezei's suggestion,[34] we have developed a Monte Carlo code for grand canonical and grand isoshear ensemble simulations of water and aqueous solutions including hydrated clay minerals. The method was validated using simulations of both pure SPC/E water and a Cs–montmorillonite clay. Results indicate that the MC approach is significantly more efficient than our previously developed MD method.[36]

A series of grand isoshear ensemble MC simulations was used to determine the free energy, energy, and entropy of clay swelling as a function of interlayer ion size and charge. The model properly predicts the relative stabilities of one- and two-layer hydrates for Cs–, Na–, and Sr–montmorillonites. Several results were consistent with a picture that ion hydration energies dominate observed swelling behavior. First, disjoining pressures were found to be correlated with ion hydration numbers. This suggests that high swelling pressures result from hydrated ion "pillars" that push the clay layers apart. The ease of formation of these pillars is correlated with ion hydration energies. Furthermore, decomposition of swelling free energies into energetic and entropic components indicates that energetic effects

dominate the swelling process, with entropy playing an important yet smaller compensating role. Finally, comparison of ion density profiles in two-layer hydrates of the three clays revealed an increasing tendency for formation of outer-sphere complexes as ion hydration energy increased.

Hysteresis in clay swelling processes is readily associated with trapping in metastable swelling states. This was illustrated using a pressure-driven compression and expansion cycle, but a similar mechanism likely accounts for hysteresis in adsorption isotherms where swelling is driven by changes in the water chemical potential.[28] Ion exchange processes on clays also show hysteresis[53] that may originate ultimately from a similar mechanism. Further work is currently underway to address this issue.

To date, most computer simulations of smectite clay properties have been performed near room temperature and pressure, where experimental knowledge is abundant. Extension of simulation investigations to more extreme conditions of either geological or industrial relevance is highly desirable. Simulations may be readily adapted to meet this objective. For example, the swelling entropies and disjoining pressures presented in this paper can be combined with an adsorption isotherm measurement to predict both the temperature and pressure dependence of clay swelling. Such predictions are likely to prove useful given the now well-established reliability of simulations under ambient conditions.

ACKNOWLEDGMENT

[1] P. J. Coughtrey and M. C. Thorne, *Radionuclide Distribution and Transport in Terrestrial and Aquatic Ecosystems* (Balkema, Rotterdam, 1983), Vol. 1.
[2] S. Staunton, Eur. J. Soil. Sci. **45**, 409 (1994).
[3] J. J. W. Higgo, Prog. Nucl. Energy **19**, 173 (1987).
[4] R. Pusch, Clay Miner. **27**, 353 (1992).
[5] C. Durand *et al.*, Rev. Inst. Fr. Pet. **50**, 187 (1995).
[6] R. W. Mooney, A. G. Keenan, and L. A. Wood, J. Am. Chem. Soc. **74**, 1371 (1952).
[7] R. Calvet, Ann. Agron. **24**, 77 (1973).
[8] M. H. Fu, Z. Z. Zhang, and P. F. Low, Clays Clay Miner. **38**, 485 (1990).
[9] F. Zhang, Z. Z. Zhang, P. F. Low, and C. B. Roth, Clay Miner. **28**, 25 (1993).
[10] I. Bérend *et al.*, Clays Clay Miner. **43**, 324 (1995).
[11] J. M. Cases *et al.*, Clays Clay Miner. **45**, 8 (1997).
[12] L. Yan, P. F. Low, and C. B. Roth, J. Colloid Interface Sci. **182**, 417 (1996).
[13] C. T. Chiou and D. W. Rutherford, Clays Clay Miner. **45**, 867 (1997).
[14] S. J. Chipera, J. W. Carey, and D. L. Bish, Adv. X-Ray Anal. **39**, 713 (1997).
[15] D. A. Laird, Clays Clay Miner. **47**, 630 (1999).
[16] W. Xu, C. T. Johnston, P. Parker, and S. F. Agnew, Clays Clay Miner. **48**, 120 (2000).
[17] N. T. Skipper, F.-R. C. Chang, and G. Sposito, Clays Clay Miner. **43**, 285 (1995).
[18] A. Delville, J. Phys. Chem. **99**, 2033 (1995).
[19] B. J. Teppen *et al.*, J. Phys. Chem. B **101**, 1579 (1997).
[20] F.-R. C. Chang, N. T. Skipper, and G. Sposito, Langmuir **13**, 2074 (1998).
[21] D. E. Smith, Langmuir **14**, 5959 (1998).
[22] R. M. Shroll and D. E. Smith, J. Chem. Phys. **111**, 9025 (1999).
[23] D. A. Young and D. E. Smith, J. Phys. Chem. B **104**, 9163 (2000).
[24] M. Chávez-Páez, K. V. Workum, L. de Pablo, and J. J. de Pablo, J. Chem. Phys. **114**, 1405 (2001).
[25] M. Chávez-Páez, L. de Pablo, and J. J. de Pablo, J. Chem. Phys. **114**, 10948 (2001).
[26] R. Sutton and G. Sposito, J. Colloid Interface Sci. **237**, 174 (2001).
[27] E. J. M. Hensen, T. J. Tambach, A. Bliek, and B. Smit, J. Chem. Phys. **115**, 3322 (2001).
[28] E. J. M. Hensen and B. Smit, J. Phys. Chem. B **106**, 12664 (2002).
[29] V. Marry, P. Turq, T. Caratiller, and D. Levesque, J. Chem. Phys. **117**, 3454 (2002).
[30] V. Marry and P. Turq, J. Phys. Chem. B **107**, 1832 (2003).
[31] O. F. Zaidan, J. A. Greathouse, and R. T. Pabalan, Clays Clay Miner. **51**, 372 (2003).
[32] M. P. Allen and D. J. Tildesley, *Computer Simulation of Liquids* (Oxford University Press, Oxford, 1987).
[33] D. Frenkel and B. Smit, *Understanding Molecular Simulation* (Academic, New York, 1996).
[34] M. Mezei, J. Chem. Phys. **112**, 1059 (2000).
[35] H. J. C. Berendsen, J. R. Grigera, and T. P. Straatsma, J. Phys. Chem. **91**, 6269 (1987).
[36] R. M. Shroll and D. E. Smith, J. Chem. Phys. **110**, 8295 (1999).
[37] N. T. Skipper, K. Refson, and J. D. C. McConnell, Clay Miner. **24**, 411 (1989).
[38] N. T. Skipper, K. Refson, and J. D. C. McConnell, J. Chem. Phys. **94**, 7434 (1991).
[39] G. W. Brindley and G. Brown, *Crystal Structures of Clay Minerals and Their X-Ray Identification* (Mineralogical Society, London, 1980).
[40] D. E. Smith (unpublished).
[41] S. W. de Leeuw, J. W. Perram, and E. R. Smith, Proc. R. Soc. London, Ser. A **373**, 27 (1980).
[42] M. Mezei, Mol. Phys. **61**, 565 (1987).
[43] J. C. Shelley and G. N. Patey, J. Chem. Phys. **102**, 7656 (1995).
[44] J. Hermans, A. Pathiaseril, and A. Anderson, J. Am. Chem. Soc. **110**, 5982 (1988).
[45] Y. Guissani and B. Guillot, J. Chem. Phys. **98**, 8221 (1993).
[46] D. J. Diestler, M. Schoen, J. E. Curry, and J. H. Cushman, J. Chem. Phys. **100**, 9140 (1994).
[47] P. Bordarier, B. Rousseau, and A. H. Fuchs, J. Chem. Phys. **106**, 7295 (1997).
[48] N. T. Skipper, A. K. Soper, and J. D. C. McConnell, J. Chem. Phys. **94**, 5751 (1991).
[49] N. T. Skipper, A. K. Soper, and M. V. Smalley, J. Phys. Chem. **98**, 942 (1994).
[50] N. T. Skipper *et al.*, J. Phys. Chem. **99**, 14201 (1995).
[51] H. Qian and J. J. Hopfield, J. Chem. Phys. **105**, 9292 (1996).
[52] K. Sharp, Protein Sci. **10**, 661 (2001).
[53] K. Verburg and P. Baveye, Clays Clay Miner. **42**, 207 (1994).